Identification of execution modes in the extrinsic apoptosis signaling network via Bayesian inference methods

Michael A. Kochen[1], Carlos F. Lopez[1,2,*]

[1] Department of Biomedical Informatics, Vanderbilt University, Nashville, TN

[2] Department of Biochemistry, Vanderbilt University, Nashville, TN

Abstract

Characterization of signal execution dynamics within complex biochemical networks is a highly challenging problem yet necessary to understand how cells process signals and commit to a biological phenotype. The mechanistic interpretation of experimental results can often be misinterpreted due to limited available data or the need for an unrealistic number of experimental measurements. Mathematical models of biochemical networks have emerged as an alternative to complement experiments and explore signal execution mechanisms. However, traditional computational methods require either detailed knowledge of model parameters or sufficient data to calibrate models to experiments, both of which can be difficult to obtain. To address this challenge, we have taken a probabilistic approach to the analysis of network-driven biochemical processes. In this work, we apply a Bayesian multimodel inference formalism to identify how relevant pathways and subnetworks contribute to the overall mechanism of a biochemical signaling network. We focus this approach on the signal execution pathways of mammalian extrinsic apoptosis. We study the effect of changing concentrations of key apoptosis regulators such as XIAP, which governs the phenotypic mode of apoptotic execution, either via the mitochondria independent (Type I) or dependent (Type II) pathways. Several hypotheses were generated regarding (*i*) differential pathway regulation by XIAP; (*ii*) apoptotic signal arrest through the caspase-only pathway; and (*iii*) the primary signal amplification concomitant with XIAP inhibition leads to signal amplification via mitochondrial involvement. Our findings substantiate the use of probabilistic and multimodel inference-based approaches for the hypotheses exploration regarding the mechanisms of signal execution dynamics. We expect that these approaches could help identify key pathways in complex networks and, in turn, accelerate testable hypothesis generation.

Author summary

Signaling dynamics within complex biochemical networks are remarkably difficult to characterize. Mathematical models are often used, in conjunction with experimentation, to explore the effect of changes in regulatory proteins on signal propagation. However, Mathematical models are often limited by a lack of knowledge regarding reaction rates and the

lack of available data to calibrate them. To overcome this issue, we have taken a probabilistic approach over parameter space that enables reaction topology and protein concentration exploration within a Bayesian evidence context. The mechanisms of signaling dynamics and the effects of perturbations in protein concentrations can thus be hypothesized in the absence of explicit reaction rates. The method is demonstrated on a model of the extrinsic apoptosis network to explore the key drivers of Type I vs Type II signal execution. Key regulators that govern the signaling phenotype of this network are modulated and changes in the apoptotic signal through the network are analyzed. In addition to supporting established experimental results, we generate novel hypotheses regarding phenotypic control and the roles of various components of this system are made.

Introduction

Emergent behaviors of complex biological networks are difficult to characterize [1, 2]. They arise from the interplay between various components and pathways that make up the larger system and because they appear only when those pieces are brought together, determining the role of any singular part can pose a significant challenge. An especially difficult behavior to study is the evolution of signal execution dynamics under changing regulatory conditions. Such analysis is essential to the identification of regulatory elements that shift signal transduction between pathways or those with the potential to elicit phenotype transitions. To study the myriad possible cellular regulatory conditions and accelerate the formation of predictive hypotheses, computational modeling is often used alongside experimental methods [3]. Such an approach was taken by Aldridge *et al.* [4] to study phenotypic regulation of the extrinsic apoptosis network. They used a kinetic model in conjunction with Lyapunov exponent based bifurcation diagrams to produce a separatrix which defines a boundary between phenotypes on the space of regulatory element concentrations. With this, they predicted that the expression of a Type I or II extrinsic apoptosis phenotype (defined as independent and dependent of the mitochondria respectively) depends on the concentration of the apoptosis inhibitor XIAP and its target Caspase-3. Raychaudhuri and Raychaudhuri [5] also focused on the Type I/II execution modes and used Monte Carlo simulations of an extrinsic apoptosis model to evaluate the effect of various model perturbations on network dynamics. Their primary conclusion was that the Type I phenotype was the result of a deterministic signaling process while the Type II phenotype was stochastic in nature.

Nevertheless, comparison of various subnetworks or pathways that represent different phenotypes using traditional physicochemical modeling is problematic. Such models depend on reaction rate parameters that are typically unknown and thus must be calibrated to experimental data – data that is often scarce [6]. Moreover, data sufficient for model calibration and the attainment of reasonable simulated outcomes may not be sufficient for the analysis of the inner dynamics of a biochemical network. Calibration of a complex model to inadequate data can result in equally good fits for very different parameter sets [7], which could potentially lead to inconsistent conclusions regarding signal flow through various components the network. To overcome these limitations, we have taken a probabilistic

approach to the analysis of differential pathway regulation and phenotype selection by utilizing methods from the field of model selection and multimodel inference [8, 9]. Our goal is to explore the overall system dynamics through the comparison of dynamics for all relevant subnetworks and make predictions regarding apoptotic signal execution and phenotypic selection under varying regulatory conditions. For that we require an algorithm to compare these subnetworks under varying regulatory conditions. Many model comparison algorithms, such as the popular Akaike information criterion (AIC) [10] and Bayesian information criterion (BIC) [11], typically use maximum likelihood formalisms to estimate the fit of a model to data. Unfortunately, kinetic biological models with different network topologies can often yield comparable calibration maximum likelihood outcomes, thus rendering these approaches unsuitable [12]. Other approaches integrate a likelihood function over all relevant parameter space, resulting in an estimate of the marginal likelihood, or model evidence, which provides a relative measure of model fit. In Eydgahi et al. [12] this was done with thermodynamic integration [13], an MCMC method, to choose between two proposed models of mitochondrial outer membrane permeabilization (MOMP). Although this approach can be accurate, it requires significant computational resources, which can pose a challenge for general use. Recently, nested sampling approaches have emerged as a more efficient alternative for evidence calculation but, to date, seldom used in biology. Here, we employ an implementation of this approach to decompose the dynamics of a signaling network and understand the effects of signal modulators in apoptosis execution [14, 15, 16].

In this work we describe the use of Bayesian multimodel inference methods to explore network dynamics across regulatory conditions and demonstrate its efficacy in the analysis apoptosis execution. The novel software pipeline used for model construction, evidence calculation, and model simulation are described in detail for mechanism exploration. Following the examples set by Aldridge et al. [4] and Raychaudhuri and Raychaudhuri [5] we test our approach toward understanding the execution and dynamics of the extrinsic apoptosis reaction network. Two complementary approaches are used. First, we employ a multimodel inference approach and deconstruct the extrinsic apoptosis reaction model (EARM) [17] model into several subnetworks, all of which carry the apoptotic signal from initial ligand cue to PARP cleavage response. The Bayesian evidence for each of these subnetworks is calculated, using an objective function that estimates the signal flow, over increasing quantities of the apoptosis inhibitor XIAP. Differential effects elicited by XIAP on the various subnetworks become apparent in the trends in evidence as XIAP is increased. The differences in these trends, representing changes in signal flow, then allow for hypotheses to be made on the underlying mechanisms of signal execution. Secondly, in a pathway targeted approach, the full extrinsic apoptosis model is retained but the evidence trends are calculated using objective functions describing the chemical flux through the caspase and mitochondrial pathways, as well as the total flux through the model. These trends are compared to one another and to the results from the multimodel inference approach to compile a complete mechanistic hypothesis of signal execution dynamics as well as how these dynamics change as the apoptotic inhibitor XIAP is increased. Lastly, we consider the trade-off between computational cost and precision by considering the number of required evaluations, the estimated error, and the estimated CPU time as the sampling population is increased. To the best of our knowledge, this is the first attempt at a truly systems

description of signal execution using a probabilistic approach and multimodel inference methods.

Methods

Modeling and simulation

The base model used here is a modified version of the Extrinsic Apoptosis Reaction Model (EARM) from Lopez et al. [17]. The modified model recapitulates extrinsic apoptosis execution to experimental data [18] upon calibration to time-dependent trajectories of Bid, Smac, and PARP (Supplementary Figure 1 Supplementary Table S1). A description of signal flow through the various components of this model is detailed in Box 1 below. The various sub-models were written in the format of PySB, a rule-based system for constructing and simulating physicochemical models under mass-action kinetics [17]. All simulations were run, in the context of Bayesian evidence estimation, using the PySB software (http://pysb.org/). All representative models and software are distributed with open-source licensing and can be found in the GitHub repository https://github.com/LoLab-VU/Bayesian_Inference_of_Network_Dynamics.

Bayesian evidence estimation

Bayesian evidence is the probability of obtaining a set of data given a particular model. It is expressed as

$$P(D|M) = \int L(D|\theta, M)\, P(\theta|M)\, d\theta \tag{1}$$

Where M is the model under consideration, D is the data, θ is a particular set of parameter values, $L(D|\theta)$ is the likelihood function describing the fit of the data to the model under those parameter values, and $P(\theta|M)$ is the prior distribution of parameters. Note that this also represents the expected value of the likelihood function on the prior distribution. All evidence estimates were made using nested sampling; introduced by Skilling in [14]. This method simplifies the evidence calculation by introducing a prior mass element $dX = P(\theta|M)\, d\theta$ that is estimated by $(X_{i-i} - X_i)$ where $X_i = e^{-i/N}$, i is the current iteration of the algorithm, and N is the total number of live points. The evidence is then written as

$$Z = \int_0^1 L\, dX \approx \sum_{i=1} L_i (X_{i-1} - X_i) \tag{2}$$

Initialization of the algorithm is carried out by randomly selecting an initial population of parameter sets (points in parameter space) from the prior distribution, scoring each one with the likelihood function, and ranking them from L_{high} to L_{low}. At each iteration of the algorithm a new set of parameter values is selected and scored. If that score is higher than L_{low}, then it is added to the population, at the appropriate rank, and L_{low} is removed from the population and added to the evidence sum (2).

Nested sampling software

All evidence estimates in this work are calculated with MultiNest, a nested sampling-based algorithm designed for efficient evidence calculation on highly multimodel posterior distributions [15, 16]. MultiNest works by clustering the live points (population of parameter sets) and enclosing them in ellipsoids at each iteration. The enclosed space then constitutes a reduced space of admissible parameter sets. This lowers the probability of sampling from low likelihood areas and evaluating points that will only be discarded. The evidence estimate is accompanied by an estimate of the evidence error. The algorithm terminates when the presumed contribution of the highest likelihood member of the current set of live points, $L_{high}X_i$ is below a threshold. Here, we use a threshold of 0.0001 and a population size and 16,000 unless otherwise noted. See [15, 16], for more details on the MultiNest algorithm. We use MultiNest with the Python wrapper PyMultiNest [19], which facilitates the integration of PySB into the nested sampling pipeline.

Objective functions

In this work we will present two methodologies that use trends in evidence values, as regulatory conditions are varied, to make inferences on changing network dynamics. We note that our choice for objective function is not a true likelihood but is interpreted in a similar manner – a higher value is indicative of a better fit to the expected outcome [20]. Both methods incorporate objective functions that represent complete apoptosis of the cell.

Multimodel inference method. In the multimodel inference method we break down the network into various subnetworks and test each, over increasing values of the apoptosis inhibitor XIAP, for efficacy in achieving apoptosis. A proxy for apoptosis in this model, and the objective function for the nested sampling calculation, is the proportion of the protein PARP that has been cleaved by caspase-3 at the end of the in-silico experiment (Supplementary Figure 1). The function is thus

$$Obj_{multimodel} = \frac{cParp}{tParp}$$

where $cParp$ is the amount of PARP that has been cleaved and $tParp$ is the total amount of PARP in the system. The evidence calculation thus provides an estimate of the average PARP cleavage over the chosen parameter ranges.

Pathway targeted method. In the pathway targeted method we again vary the regulator XIAP but retain the full model while using targeted objective functions that represent the chemical flux through different pathways in the network similar to [21]. We consider the signal flux through the caspase pathway, the mitochondrial pathway and the total flux through the network. The objective function estimating signal flux through a pathway is

$$Obj_{pathway} = \sum_{t=0}^{T} \frac{\sum_0^t C3_{pathway}}{\sum_0^t C3_{total}} \times (cParp_t - cParp_{t-1})$$

where t represents time in seconds, $\frac{\sum_0^t C3_{caspase}}{\sum_0^t C3_{total}}$ is the proportion of total currently active caspace-3 that was produced in the pathway at time t, and $(cParp_t - cParp_{t-1})$ is the total PARP that has been cleaved by Caspase-3 between times $t-1$ and t. The evidence calculation in this case estimates the average flux through the target pathway over the chosen parameter ranges.

Parameter ranges and initial conditions

The prior distribution takes the form of a set of parameter ranges, one for each reaction rate parameter. The chosen ranges span four orders of magnitude around generic reaction rates deemed plausible [22] and are specific to the type of reaction taking place. The ranges of reaction rate parameters, in Log_{10} space, are 1st order forward: [-4.0, 0.0], 2nd order forward: [-8.0, -4.0], 1st order reverse: [-4.0, 0.0], catalysis: [-1.0, 3.0]. These ranges were also used in calibration of the base model. Initial conditions were either gleaned from the literature [23, 24] or taken from a previous model of extrinsic apoptosis [17]. Because the baseline model was designed to concur with Type II apoptotic data (see above), literature derived initial conditions were based on Type II Jurkat or Hela cell lines.

Bayes factor Landscape construction

Evidence estimates are often used to select between two competing models by calculating the Bayes factor, or the ratio of their evidence values. This provides a measure of confidence for choosing one model over another. We can likewise use trends in evidence values to produce trends in Bayes factors that provide additional insights into the dynamical relationship between pathways. To facilitate construction of Bayes factor trends with a continuous and symmetric range, the Bayes factors were calculated as

$$Bf = \begin{cases} -\frac{Z_2}{Z_1} + 1 \;\; if \; Z_1 < Z_2 \\ \frac{Z_1}{Z_2} - 1 \;\; if \; Z_1 > Z_2 \end{cases}$$

where Z_1 and Z_2 are the evidence estimates for two pathways under comparison.

Computational resources

Because of the high computational workload necessary for this analysis, a wide range of computational resources were used. The bulk of the work was done on the ACCRE cluster at Vanderbilt University leveraging up to 600 compute nodes running Intel Xeon processors and a Linux OS (www.vanderbilt.edu/accre/). As many as 300 evidence estimates were run in parallel on this system. Additional resources included two local servers, also running Intel processors and a Linux OS, as well as a small local four node cluster running Linux and AMD Ryzen 1700 processors. A detailed breakdown of CPU time can be found in the results section.

Box 1: Schematic of apoptotic signal flow through the Extrinsic apoptosis network.

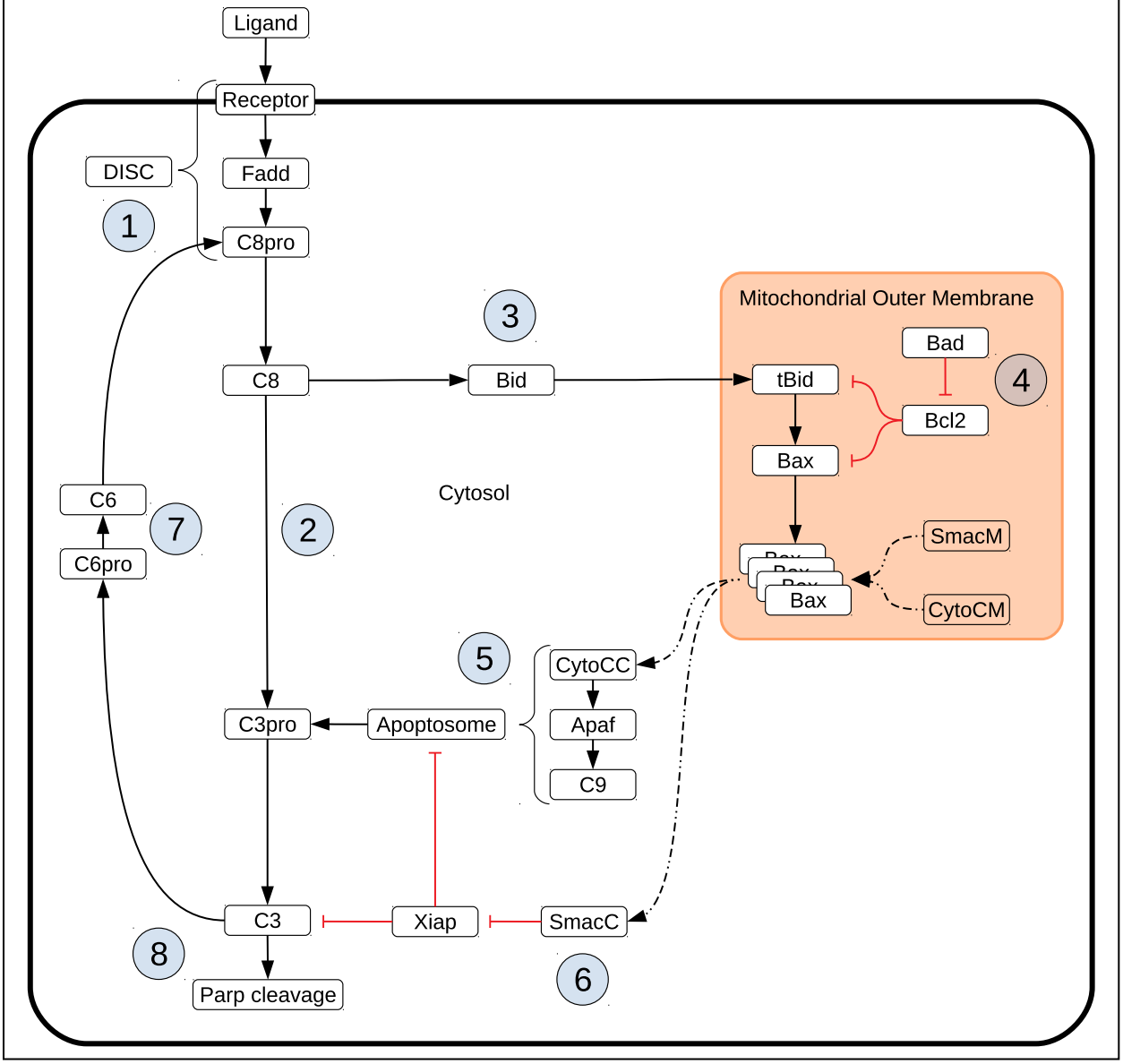

Extrinsic apoptosis execution. Extrinsic apoptosis is a receptor mediated process for programmed cell death. It's initiated when a death inducing member of the tumor necrosis factor (TNF) superfamily of receptors (FasR, TNFR1, etc.) is bound by its respective ligand (FasL, TNF-α, etc.), setting off a sequence biochemical events that result in the orderly deconstruction of the cell [28]. The first stage of this sequence is the assembly of the DISC at the cell membrane ① and the subsequent activation of Caspase-8. Upon ligand binding and oligomerization of a receptor such as FasR or TRAIL, an adapter protein, like FADD (Fas-associated protein with death domain), is recruited to the receptors cytoplasmic tail [29, 30, 31]. FADD, in turn, recruits Caspase-8 via their respective death effector domains (DEDs), thus completing DISC formation [30, 31]. Other DISC components could also be included here, such as the regulator cFlip [32]. Once recruited, proximal Procaspase-8 monomers dimerize, inducing their autoproteolytic activity and producing active Caspase-8 [33, 34, 35].

After Caspase-8 activation the apoptotic signal can progress down two distinct pathways that both lead to the activation of Caspase-3 and the ensuing proteolysis of downstream targets. One pathway consists of a caspase cascade in which active Caspase-8 directly cleaves and activates Caspase-3 ② [36], while another, more complex pathway is routed through the mitochondria. In the mitochondrial pathway Caspase-8 cleaves the pro-apoptotic Bcl-2 family protein Bid in the cytosol, which then migrates to the mitochondria ③ where it initiates mitochondrial outer membrane permeabilization (MOMP) and the release of pro-apoptotic factors that lead to Caspase-3 activation [37, 38].

MOMP has its own set of regulators that govern the strength of apoptotic signaling through the mitochondria ④. After Caspase-8 activated Bid, (tBid), migrates to the mitochondria it activates proteins in the outer mitochondrial membrane, such as Bax, that subsequently self-aggregate into membrane pores and allow exportation of Cytochrome-c and Smac/DIABLO to the cytosol [39]. Bid and Bax are examples of pro-apoptotic proteins from the Bcl-2 family, all of which share BH domain homology [40]. Other members of this family act as MOMP regulators; the anti-apoptotic Bcl-2, for example, binds and inhibits both Bid and Bax while the pro-apoptotic Bad similarly binds and inhibits its target, Bcl-2 [41, 42, 43, 44]. Many other pro- and anti-apoptotic members of the Bcl-2 family have been discovered and together regulate MOMP [45].

Regardless of which pathway is chosen, the intermediate results are Caspase-3 activation and subsequent cleavage of PARP ⑧, a proxy for cell death in the analyses here [46, 47]. XIAP (X-linked inhibitor of apoptosis protein) is an inhibitor of Caspase-3 and has been proposed to be a key regulator in determining the apoptotic phenotype of a cell (Type I/II cells are, respectively, independent/dependent on the mitochondrial pathway) [48]. XIAP sequesters Caspase-3 but also contains a ubiquitin ligase domain that directly targets Caspase-3 for degradation. The inhibitor also sequesters and inhibits the Caspase-3 activating Caspase-9 residing within the apoptosome complex [49, 50, 51]. Apoptosome formation is initiated by Cytochrome-c exported from the mitochondria during MOMP ⑤. Cytochrome-c induces the protein APAF-1 to oligomerize and subsequently recruit and activate Caspase-9, thus forming the complex [52]. Another MOMP export, the protein Smac/DIABLO ⑥, binds and inhibits XIAP, working in tandem with Cytochrome-c to oppose XIAP and carry out the apoptosis inducing activity of the Type II pathway [53]. Finally, Procaspase/Caspase-6 constitutes a feed forward loop between Caspase-3 and Caspase-8 ⑦ [54].

Results

General Strategy

To investigate the dynamics of apoptosis execution in the EARM, we take a model selection and multimodel inference approach and investigate how network components describe signal execution. The final goal is to build a composite description of system dynamics by observing variations in signal throughput between these subnetworks relative to changes in regulatory conditions. This differs from traditional model selection and multimodel inference applications. A more typical use of these methods when dealing with physicochemical models is to rank a set of proposed models based on their fit to experimental data [12, 25, 26, 27]. High ranking models could then be averaged to obtain a composite model [8, 9]. Nevertheless, whether the analysis targets model structure (fit to data) or dynamics (fit to expected outcomes), a quantity such as the estimated Bayesian evidence indicates a more robust working range of parameters and a more likely model for higher evidence values [12]. It should be noted that the evidence calculation also inherently penalizes model complexity because models with higher parameter counts are integrated over a higher dimensional space [14].

Our general approach to use Bayesian evidence calculations and characterize network execution modes is shown schematically in Figure 1. Two complementary methods are used. In a multimodel inference approach the model is deconstructed into biologically relevant components and the evidence is evaluated relative to the desired simulation outcome. If we tailor the objective function to represent the strength of signal execution, as measured by cleaved PARP at the end of the simulation run, then the evidence describes the likelihood that the signal is effectively transmitted through the network. Comparison of the change in signal strength through relevant subnetworks, subsequently allows for inferences to be made on the effect of both the perturbed network regulator as well as various network components on the overall dynamics of the system. We use these trends in Bayesian evidence to examine how XIAP alters the dynamics of the extrinsic apoptosis (Box 1) and gain insight into the mechanisms that commit the network to either Type I (mitochondria independent) or II (mitochondria dependent) execution modes. The EARM reaction topology was deconstructed into six relevant network variations (Figure 2A-F). These include the full model, the caspase pathway, and the mitochondrial pathway including two subpathways that either directly transduce the apoptotic signal (via Caspase-3 cleavage) or inhibit XIAP, the inhibitor of activated Caspase-3 (and Caspase-9 in the Apoptosome). Also included are combinations of the caspase pathway with either of the two mitochondrial subpathways and the mitochondrial signal transduction pathway in isolation. A model for each network variation and each initial value of XIAP was encoded in PySB and each model was evaluated using the MultiNest algorithm via the PyMultiNest Python wrapper as described in the Methods section [15, 16, 19].

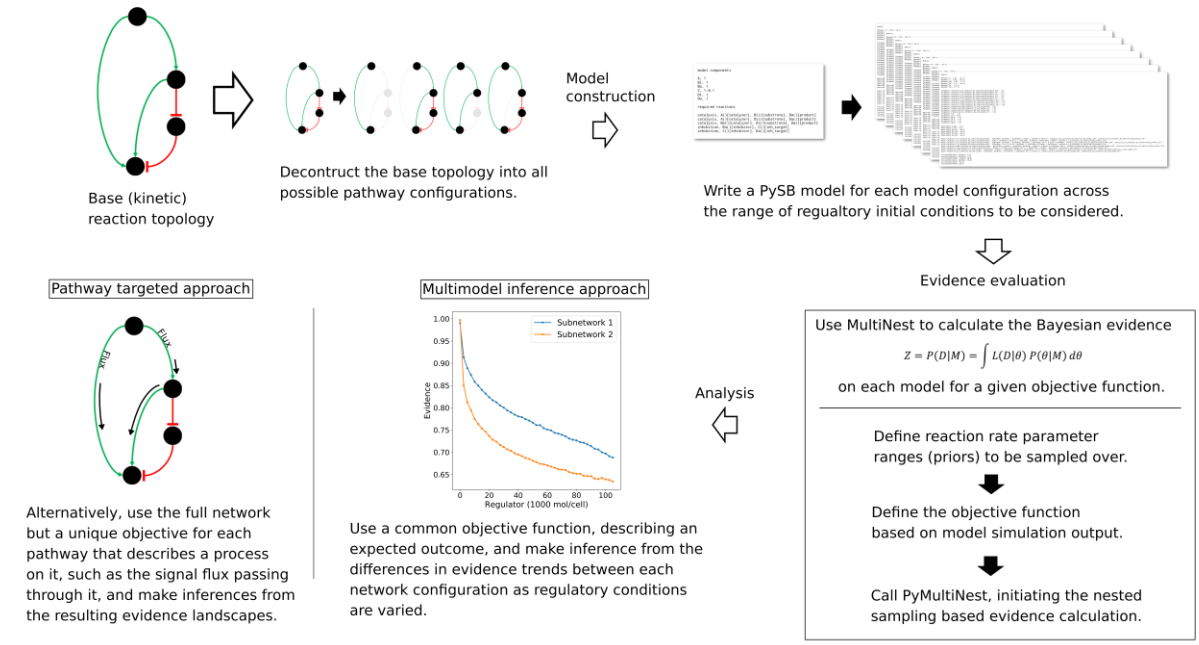

Figure 1. General workflow for the analysis of network dynamics using trends in Bayesian evidence. The target network is first deconstructed into all relevant subnetworks. A model for each subnetwork and each incrementing set of regulatory conditions is then created and passed to an algorithm for estimation the Bayesian model evidence. The evidence is calculated on a user-defined objective function, describing signal transduction through the network, and over a range of parameter values (the prior). The evidence trends over changing regulatory conditions are then compared to make qualitative inferences regarding network dynamics. In an alternative method, the full model is retained, but the objective function is targeted to different pathways. Inferences on network dynamics can again be made from the trends in the evidence calculations.

We then take a pathway targeted approach and, while retaining the complete network, report trends in Bayesian evidence using objective functions that measures apoptotic signal flux (see Methods for details) through both the caspase and mitochondrial pathways, as well as the total flux through the network. Both XIAP and the mitochondrial apoptosis inhibitor Bcl-2 were varied to form evidence landscapes that were used, along with the trends from the multimodel inference approach, to make predictions about changing network dynamics under regulatory perturbations.

Taken together, we expect that these two approaches for the decomposition of signal execution into network components will provide a systems-level understanding of how the dynamics of signal execution are affected by changes in regulator concentrations and allow predictions on signaling outcomes to be generated.

Differential downregulation of extrinsic apoptosis subnetworks by XIAP

XIAP has been put forth as a critical regulator in the choice of apoptotic phenotype. In Jost et al. [48] they examined hepatocytes (Type II cells) and lymphocytes (Type I cells) under different conditions to examine the role XIAP plays in Type I/II determination and made several observations. They reported that Fas ligand (FasL) induced apoptosis resulted in increased levels of XIAP in hepatocytes but lowered levels in thymocytes. They then found that while XIAP deficient mice died earlier than wild-type when injected with hepatocyte targeted FasL or anti-Fas antibody, XIAP deficient thymocytes showed no increase in apoptosis. From this they concluded that XIAP must be a key regulator of apoptosis in hepatocytes. Lastly, they treated XIAP, Bid, and XIAP/Bid deficient mice, along with wild-type, with FasL or Fas-antibody. All but the Bid-only deficient mice showed hepatocyte effector caspase activation, implying that the loss of XIAP rendered previously apoptosis resistant Bid-only knockouts susceptible to apoptosis through the Type I pathway. Altogether, they concluded that XIAP is the key regulator that determines the choice of pathway.

The results in Jost et al. [48] imply that the cellular level of XIAP determines the preferred apoptosis pathway with higher levels specific to Type II cells and lower levels specific to Type I. To test this hypothesis, and infer a mechanism for it, we computed the Bayesian evidence for six apoptosis-inducing subnetworks of the extrinsic apoptosis model at varying concentrations of XIAP. One of these subnetworks is the caspase pathway in isolation (Figure 2A) which represents the Type I phenotype (mitochondria-independent pathway). Also included are the caspase pathway along with either the Caspase-3 activating component (Figure 2B) or the XIAP inhibiting component (Figure 2C) of the mitochondrial pathway, as well as the isolated mitochondrial Caspase-3 activating component (Figure 2D). From these we can examine the possible contributions of these subpathways to the overall likelihood of achieving apoptosis. Finally, the full isolated mitochondrial pathway (Figure 2E) and the complete model (Figure 2F) are included. XIAP was varied from 0 to 200,000 molecules per cell in increments of 250 to explore how changes in XIAP affect the likelihood of apoptosis execution. For those networks that include components of the mitochondrial pathway Bcl-2 was excluded to ensure those components were fully active. All other initial values were fixed at the levels shown in supplementary Table S1. In the absence of XIAP all subnetworks have evidence estimates greater than 0.98 and those that include XIAP inhibition are greater than 0.99, (Figure 2G, supplementary Table S2) indicating that they all reach full PARP cleavage, and by extension apoptosis, across the allowed range of parameters.

As XIAP levels increase we see differential effects on these subnetworks in the form of diverging evidence estimates indicating differences in the efficacy of XIAP induced apoptotic inhibition. The isolated caspase pathway (Figure 2G green) shows the steepest decline which is most prominent for lower values of XIAP but diminishes as XIAP increases. The evidence trend for the caspase pathway clearly diverges from those of the rest of the subnetworks, particularly the complete model and the (complete) mitochondrial pathway. The expected value for the proportion of PARP cleavage, the average PARP cleavage over the provided parameter ranges, for the caspase pathway falls to 0.5 at an XIAP level of roughly 32,000. The complete and mitochondrial networks on the other hand require XIAP levels nearly 3x as high with the

evidence value for the complete network reaching 0.5 at around 92,000 and the mitochondrial network reaches the halfway mark at around 95,000. The Bayes factors (ratios of evidence values) average 1.205 and 1.204 over the entire range of XIAP for the complete/caspase and mitochondrial/caspase ratios respectively. The ratios tend to be higher in the first half of this range with respective averages of 1.253 and 1.278 between XIAP values of 250 and 100,000. For reference, the estimated errors for log-evidence values are on the order of 10^{-3} and are displayed in Figure S2.

The small differences in evidence values and subsequently the Bayes factors are not surprising since every subnetwork being considered is capable of transmitting the apoptotic signal. Thus, we should not expect differences of evidence that would rule out any of them under model selection criteria. In a classical model selection and multimodel inference scenario small differences in evidence estimates that would not allow for selection of a favored model might be used to construct a composite model, weighting the various components by the evidence values [8, 9]. Fortunately, we have no need to choose a best model as the complete model already represents the biology as we understand it. The goal here is to use the differences in evidence to construct a composite picture of, not the structure of the model, but signaling dynamics. For that we consider relative *changes* in the evidence values as XIAP is increased. Because the caspase pathway is representative of the Type I phenotype, the disproportionate drop in its evidence (expected proportion of PARP cleavage) as XIAP increases is consistent with experimental evidence showing XIAP induced transition to a Type II phenotype. Those networks containing the full mitochondrial subnetwork, including the isolated network and the complete network, are also affected by XIAP but clearly show a higher resistance to its anti-apoptotic effects (higher expected PARP cleavage), particularly at moderate levels of the inhibitor. This suggests a growing dependence on mitochondrial involvement in apoptosis as XIAP increases from low to moderate levels. At higher levels of XIAP the evidence trend for the caspase pathway levels off and the gap between the caspase pathway evidence trend and that for the mitochondrial and complete networks narrows. Note that the evidence values for the caspase pathway at the high end of XIAP levels are around 0.33 and level off. We do not expect to see evidence values near the theoretical minimum evidence of apoptosis value of 0 with reasonable values of XIAP. The disproportionate effect of XIAP inhibition of apoptosis on the caspase pathway suggests that the mechanism for XIAP induced transition to a Type II pathway is simply differential inhibition of the apoptotic signal through the isolated caspase pathway vs those with mitochondrial involvement.

The next two highest evidence trends belong to the networks representing caspase with mitochondrial activation of Caspase-3 and mitochondrial activation of Caspase-3 alone (Figures 2G purple and 2G brown). For most of the range with XIAP below 100,000 these two trends have largely overlapping trajectories, despite the fact that the former has twice as many paths carrying the apoptotic signal. By the time XIAP reaches a level of 100,000 the two trends diverge as the decrease in the trend for the mitochondrial activation only network accelerates. This can be explained by XIAP overwhelming the Apoptosome at these higher levels. The apoptosome is an apoptosis inducing complex (via Caspase-3 cleavage) consisting of Cytochrome C, APAF-1, and Caspase-9, and is an inhibitory target of XIAP. As XIAP increases past 125,000 the mitochondrial activation only trend falls below even the caspase only

evidence values, possibly due to the two-pronged inhibitory action of XIAP at both the Apoptosome and Caspase-3. An interesting observation here is that the addition of the caspase pathway to the mitochondrial activation pathway does not appear to increase the likelihood of achieving apoptosis for lower values of XIAP. It may be that any signal passing through the caspase pathway is quashed by XIAP until the Apoptosome becomes active, at which point it does not matter which pathway the signal takes.

Above those two trends is the trend for the network consisting of the caspase pathway and mitochondrial inhibition of XIAP (Figure 2G red). Below an XIAP level of 100,000 this trend is consistently above the trend for the network of the caspase pathway plus mitochondrial activation of Caspase-3. Note that while the caspase pathway does not appear to increase the likelihood of achieving apoptosis when added to the mitochondrial activation pathway (Figure 2G purple) the amplification of the caspase pathway via mitochondrial inhibition of XIAP leads to a higher likelihood than direct activation through the mitochondria. This suggests the possibility that the primary mechanism for mitochondrial apoptotic signal amplification may be inhibition of XIAP, with direct signal transduction a secondary mechanism. Above an XIAP level of 100,000, the caspase with XIAP inhibition trend drops to levels roughly in line with the trend for the caspase pathway plus direct activation, possibly due to the fact that Smac, the mitochondrial export that inhibits XIAP, is also set to 100,000 molecules per cell. Both, however, remain more likely to attain apoptosis than the caspase only pathway.

The two subnetworks with the highest evidence trends for apoptotic signal execution are the complete model and the isolated mitochondrial pathway (Figures 2E orange and 2F blue). As previously mentioned, both of these networks contain the full mitochondrial pathway implying that this pathway supports resistance to XIAP inhibition of apoptosis. Between XIAP levels of 0 to 100,000 the two trends track very closely, with the mitochondrial only pathway showing a slight but consistent advantage for apoptosis execution. The average difference between an XIAP level of 20,000 and 80,000 is roughly 0.014, meaning we expect the average PARP cleavage to favor the mitochondrial only pathway by about 1.4 percentage points. The average mitochondrial/complete Bayes factor for this range is only 1.024, which would typically be considered unremarkable. Context matters however, and the context here is that the complete network has potentially twice the bandwidth for the apoptotic signal, namely the addition of the more direct caspase pathway. Together, this raises the possibility that under some, likely narrow, conditions the caspase pathway is not a pathway but a sink for the apoptotic signal. In such a scenario, the signal through the caspase pathway would get lost as Caspase-3 is degraded by XIAP. Not until the signal through the mitochondrial pathway begins inhibiting XIAP could the signal proceed. Around the 100,000 level of XIAP the evidence trend for the mitochondrial pathway crosses below that for the complete network. This could be due to the parity with Smac, components of the Apoptosome, or a combination of the two.

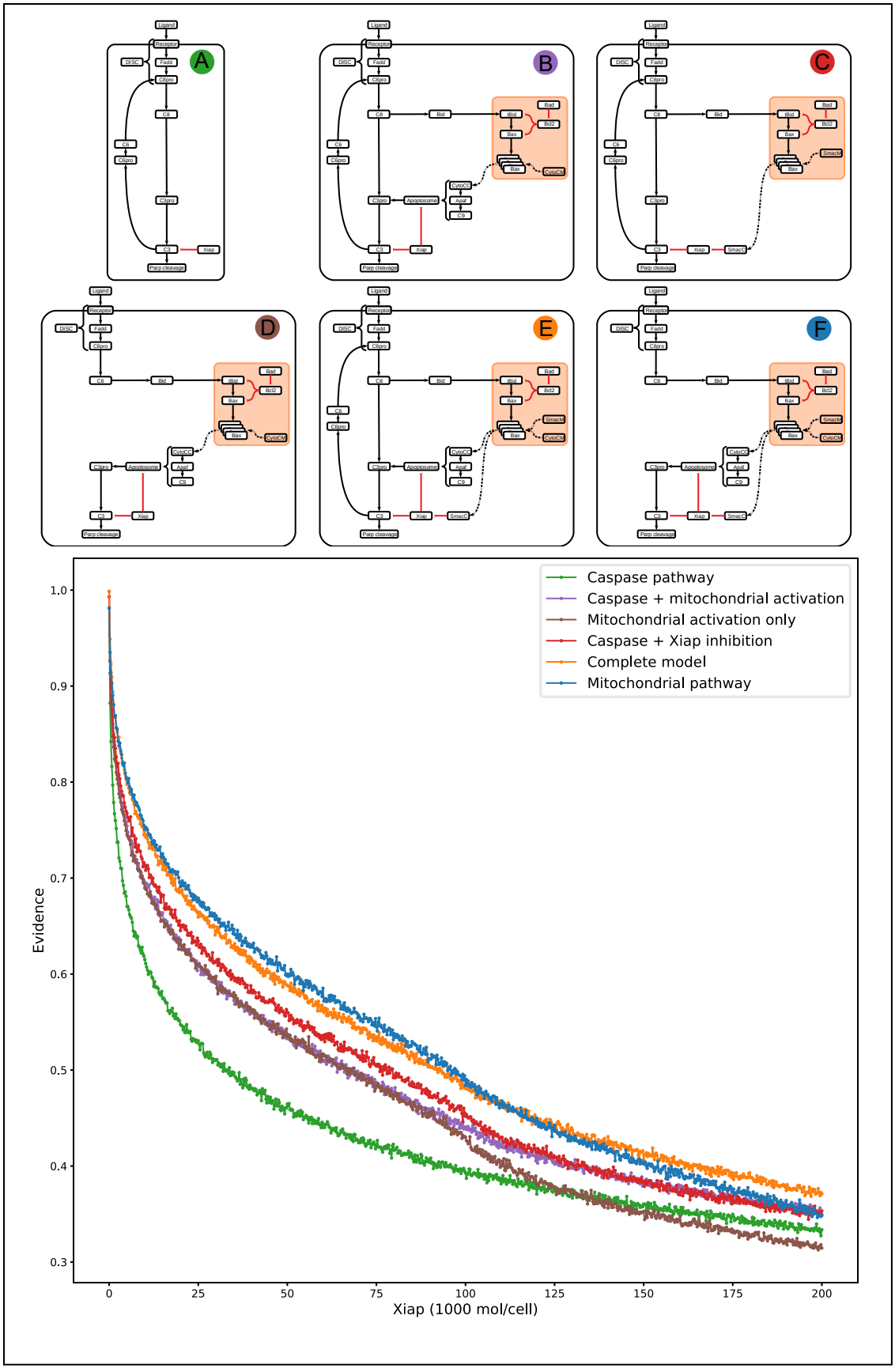

Figure 2. Extrinsic apoptosis subnetworks and Bayesian evidence for achieving apoptosis. (A) The isolated caspase pathway. (B) The caspase pathway with the Caspase-3 activating component of the mitochondrial pathway. (C) The caspase pathway with the XIAP inhibiting component of the mitochondrial pathway. (D) The isolated Caspase-3 activating component of the mitochondrial pathway. (E) The complete network. (F) The isolated mitochondrial pathway. (G) The trends in Bayesian evidence for each of the networks in (A)-(F) over a range of values the apoptosis inhibitor XIAP and for an objective function that computes the proportion of Parp cleavage (a proxy for cell death) at the end of a simulated run.

Bayes factor trends and XIAP influence on Type I/II apoptosis phenotype

Typical model selection methods calculate the evidence ratios, or Bayes factors to choose a preferred model and estimate the confidence of that choice [8, 9]. When comparing the *trends* in the evidence, the associated trends in the Bayes factors can provide additional information about changing network dynamics under regulatory perturbations. To characterize the effect of XIAP on the choice of apoptotic phenotype, Type I or II, we calculated the evidence ratios (Figure 3B), as defined in the Methods section, for each value of XIAP between the caspase pathway and both the complete network and mitochondrial pathway (Figure 2G and 3A) with a fully active mitochondrial pathway (no Bcl-2 activity). In these Bayes factor calculations, the denominator is set to the evidence for the caspase pathway so that higher values favor a need for mitochondrial involvement. An interesting feature of both the complete and mitochondrial evidence ratio trends is the peak and reversal at a moderate level XIAP. This reflects the initially intense inhibition of the caspase pathway that decelerates relatively quickly as XIAP increases, and a steadier rate of increased inhibition on networks that incorporate the mitochondrial pathway. The ratios peak between 45,000 and 50,000 molecules of XIAP, more than double the value of its target molecule Caspase-3 at 21,000, and represents the optimal level of XIAP for the requirement of the mitochondrial pathway and attainment of a Type II phenotype. Given the near monotonic decline of the evidence trends of both pathways, representing increasing suppression of apoptosis, the turn and decline in the Bayes factor landscape may represent a shift toward complete apoptotic resistance. This could be tested with more traditional kinetic modeling as was shown experimentally in Aldridge et al. [4].

A common technique to study apoptosis is to knockdown Bid, overexpress Bcl-2, or otherwise shut down MOMP induced apoptosis through the mitochondrial pathway. This strategy was used in Jost et al. [48] to study the role of XIAP in apoptosis and in the work of Aldridge et al. [4]. Taking a similar approach, we set Bcl-2 levels to 328,000 molecules per cell, in line with experimental findings [23], to suppress MOMP activity and recreated the evidence and evidence ratio landscapes (Figures 3C and 3D). Under these conditions the evidence trend for the mitochondrial pathway drops well below that of the caspase pathway which is reflected in the Bayes factor trend as a shift into negative territory, an indication that the caspase pathway is favored. The evidence trend for the complete network under MOMP inhibition is shifted closer to that for the caspase pathway but continues to be more likely to execute apoptosis throughout the range of XIAP. The peak for the associated Bayes factor trend is flattened by roughly two-thirds implying increased XIAP levels are less likely to induce a transition to a Type

II phenotype in a system with an already hampered mitochondrial pathway. Inhibition of MOMP to the point of annihilating any contribution from the mitochondrial pathway would result in uninformative mitochondrial pathway evidence values and the mitochondria/caspase ratio trend that is simply an inverted reflection of the caspase evidence trend. The evidence trend for the complete network would be indistinguishable from that for the caspase pathway alone and the complete/caspase ratio trend would simply flatline. Isolation of active biologically relevant subnetworks and direct comparison under changing conditions using trends in Bayesian evidence enables the extraction of information regarding the pathway interactions and differential network dynamics.

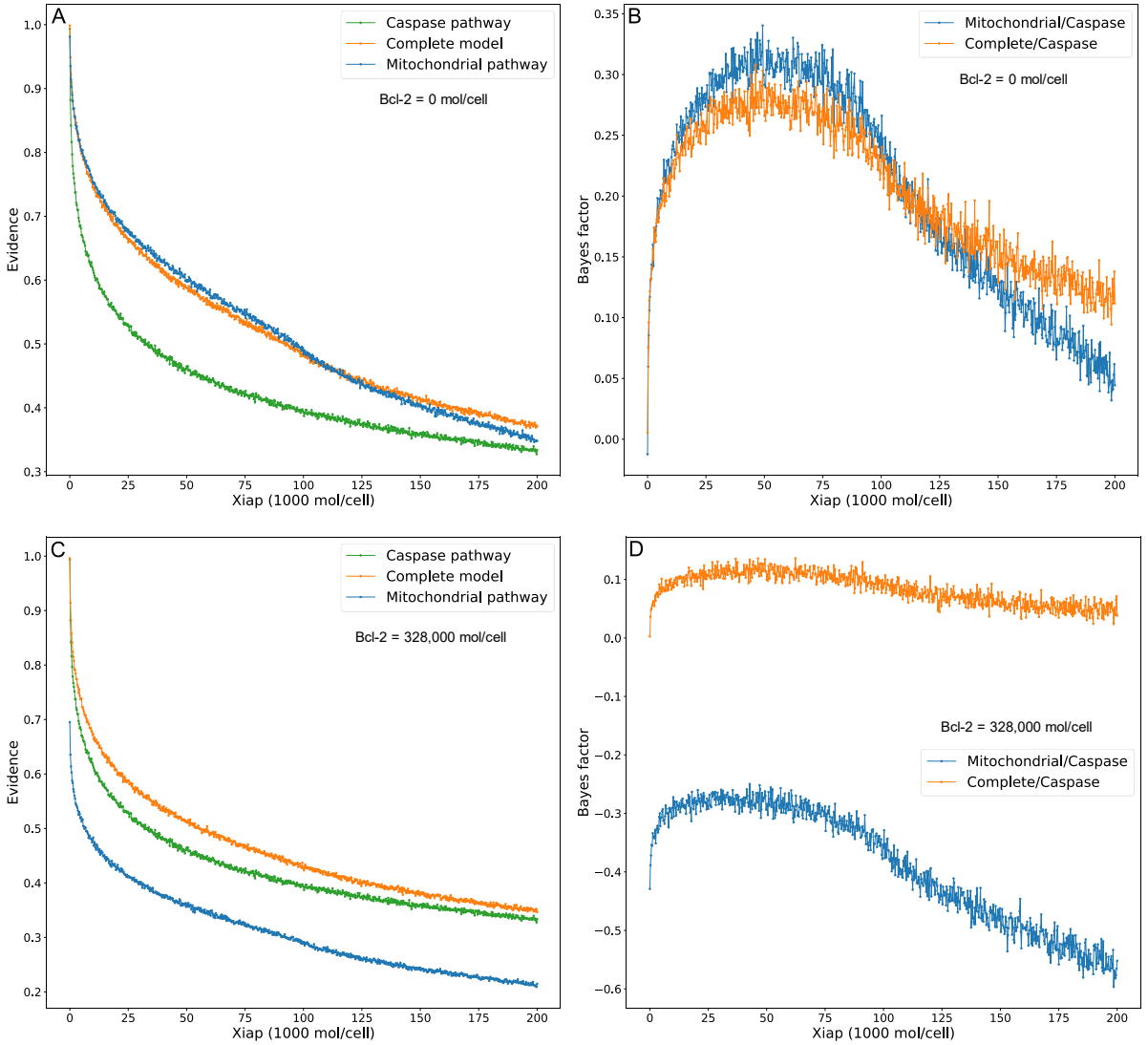

Figure 3. Evidence ratio trends under increasing levels of the apoptotic inhibitor XIAP for am inhibited and uninhibited mitochondrial pathway. (A) Evidence trends for the caspase pathway (green), mitochondrial pathway (blue), and complete network (orange) with no MOMP inhibition. (B) Trends for the mitochondria/caspase (blue) and the complete/caspase (orange) evidence ratios from the trends in (A). (C) Evidence trends for the caspase pathway (green), mitochondrial pathway (blue), and complete network (orange) with MOMP inhibitory protein BCL-2 at 328,000 mol. per cell. (D) Trends for the mitochondria/caspase (blue) and the complete/caspase (orange) evidence ratios from the trends in (C).

Caspase and mitochondrial pathway signal flux

Deconstruction of a network into all relevant subnetworks and comparison of the relative changes in the evidence for apoptosis as regulatory conditions change provides a reductionist view of how various network components interact with one another and affect the overall signaling dynamics. To get a holistic view of changes in signaling dynamics that incorporates every network component we calculate the evidence for signal flux through both the caspase and mitochondrial pathways while retaining the complete network model. Instead of considering different models with the same objective function this method considers the same network but equivalent objective functions for different pathway target. Inference of differential signal flow via calculation of pathway flux was introduced in Shockley et al. [21]. In that work they calculated the path fluxes for a number of initial conditions and over an ensemble of parameter sets. Nested sampling, along with a signal flux-based objective function, extends this idea with the calculation of the expected value for signal flux through a target pathway via integration over a parameter range. Because both pathways cleave Caspase-3, which goes on to cleave the final product PARP, the objective for each pathway was the sum, over time T in seconds, of the proportion of Caspase-3 cleaved through that pathway at time t multiplied by the amount of PARP cleaved from time t-1 to time t (see Methods). In addition to runs for both pathways an additional run for the total signal flux was carried out. We explored an XIAP concentration ranging from 0 to 100,000 molecules per cell and Bcl-2 from 0 to 200,000 molecules per cell, in increments of 2500 and 10,000 respectively, producing a 3-dimensional evidence landscape for each target objective. Because the computational cost of these objectives is significantly higher than simply calculating the proportion of cleaved PARP at the end of a simulation, the number of live points in the sampling algorithm was reduced from 16,000 to 4,000.

The evidence for signal flux through the caspase pathway showed a sharp initial decline that becomes more gradual as XIAP increases (Figure 4A). This appears to be more pronounced at the higher end of the Bcl-2 range. As Bcl-2 is increased the evidence increases, again becoming more gradual at higher levels of Bcl-2. This effect is clearly more prominent for lower levels of XIAP, likely because of the overall higher levels of signal throughput. The increase in signal flux through the caspase pathway as Bcl-2 increases is indicative of a shifting apoptotic signal from the mitochondrial to the caspase pathway; this is also evident in the decreasing mitochondrial signal flux as Bcl-2 increases (Figure 4B). As with the caspase pathway, increasing XIAP levels causes a decrease in signal flux through the mitochondrial pathway. The effects of both Bcl-2 and XIAP appear to diminish as the other increases. The combined responses to increases in XIAP and Bcl-2 for the caspase and mitochondrial pathways are evident in the evidence landscape for total flux. The total apoptotic signal flux decreases sharply as XIAP increases but remains largely stable, with only relatively small declines, as Bcl-2 is increased. Thus, while XIAP inhibits the flux through both pathways, Bcl-2, under the given simulation conditions, appears to primarily shift the flux to the caspase pathway and inhibits apoptosis to only a small degree compared to XIAP. Note that because the evidence calculations produce expected values for signal flux, the values produced for the caspase and mitochondrial pathways are additive. The average and average absolute differences between the total flux and the combined caspase and mitochondrial flux are -0.00565 and 0.00866 respectively (Supplementary Table S3).

Figure 4D displays the evidence trends for each objective over the full range of XIAP and at a Bcl-2 level of 0 for a fully active mitochondrial pathway. Throughout the range of XIAP (and Bcl-2 as well, Figures 4A and 4B), the caspase pathway retains a consistently higher expected signal flux. This supports the hypothesis that a significant proportion of the mitochondrial signal amplification is due to facilitation of the signal through the caspase pathway via XIAP inhibition and may, in fact, be the primary mechanism. Figure 4E displays the evidence trends over the range of Bcl-2 at an XIAP level of 0, which clearly shows a shift in flux from the mitochondrial to the caspase pathway. Total flux is nearly complete throughout the range, meaning that the signal results in the cleavage of nearly all available PARP. The shift in signal flux from the mitochondrial to the caspase pathway appears to be, at every level of XIAP and under these simulation conditions, the primary effect of Bcl-2. This implies that even a weak signal through the mitochondria may be enough to inhibit XIAP via SMAC and that much higher binding affinities than the given parameter ranges allowed would be required for Bcl-2 to have a substantial inhibitory effect on apoptosis. Shifting the ranges for the rates of Bcl-2:Bid and Bcl-2:Bax dissociation to [-8.0, -4.0] and [-7.0, -3.0] respectively brings the K_d values roughly in line with [55] and does indeed produce a more pronounced, but still modest, effect (Figure S3). Further adjustments of the model, both in the initial values and parameter ranges, may be necessary to elicit a higher impact from Bcl-2.

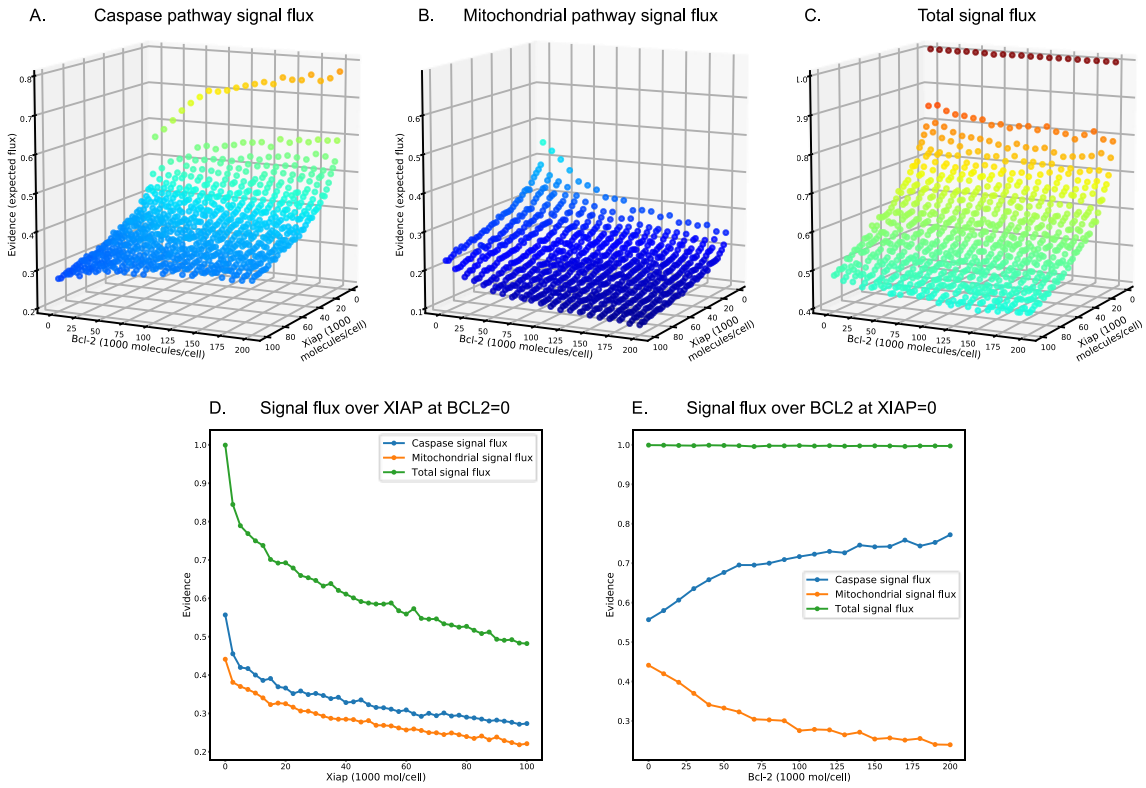

Figure 4. Apoptotic signal flux. (A)-(C) Apoptotic signal flux evidence landscapes over the apoptosis regulators XIAP (range of 0 to 100,000 molecules per cell) and Bcl-2 (range of 0 to 200,000) for (A) the caspase pathway, (B) the mitochondrial pathway and (C) the total system flux. (D) and (E) Comparison of the landscapes at a Bcl-2 and XIAP levels of 0 (D and E respectively).

Precision vs computational cost

Increasing the precision of the evidence estimates, and tightening the evidence trendlines, is accomplished by increasing the number of live points in the nested sampling algorithm. The trade-off is an increase in the number of evaluations required to reach the termination of the algorithm and an accompanying increase in total computation time. Figures 5A and 5B display the required number of evaluations for the caspase pathway and complete network at population sizes of 500, 1000, 2000, 4000, 8000, and 16,000, when run with the PARP cleavage objective function. For both models the number of evaluations roughly doubles for every doubling in population size. Of note here is the higher number of required evaluations for the lower parameter model. The caspase pathway has only 22 parameters and required an average of 64,612 evaluations at a population size of 16,000 while the complete network, with its 56 parameters required only 53,652 evaluations, on average (Supplementary Table S4). Figures 5C and 5D are the average estimated errors calculated by the MultiNest algorithm over each population size for the caspase and complete networks respectively. As expected, error estimates fall roughly as $n^{-1/2}$ [56], signifying clear diminishing returns as the number of live points is increased. The average CPU process times, as estimated by Python's `time.clock()` method, are given in Figures 5E and 5F for the caspase and complete networks respectively. Despite the greater number of required evaluations for the caspase network the average clock times for the complete network is significantly higher. At a population of 16,000 the caspase network had an average clock time of 11,964 seconds compared to 76,981 for the complete network. The difference is due to the greater simulation time for the much larger complete model. Ultimately, the choice of population size for the methods we have laid out here will depend on the networks to be compared, the objective function, and how well the evidence trends must be resolved in order to make inferences about network dynamics. For example, at a population size of 500 the evidence trend for the caspase pathway is clearly discernable from the mitochondrial pathway and the complete network, but the latter two are largely overlapping (Figure s4A). At higher population levels, however, two distinct mitochondrial and complete trends become apparent (Figure s4K). If Bayes factor trends are desired then the choice of population size must take into consideration the amplification of the noise from both trends (see Figures s4 (B, D, F, H, J, L) for complete/caspase Bayes factor trends).

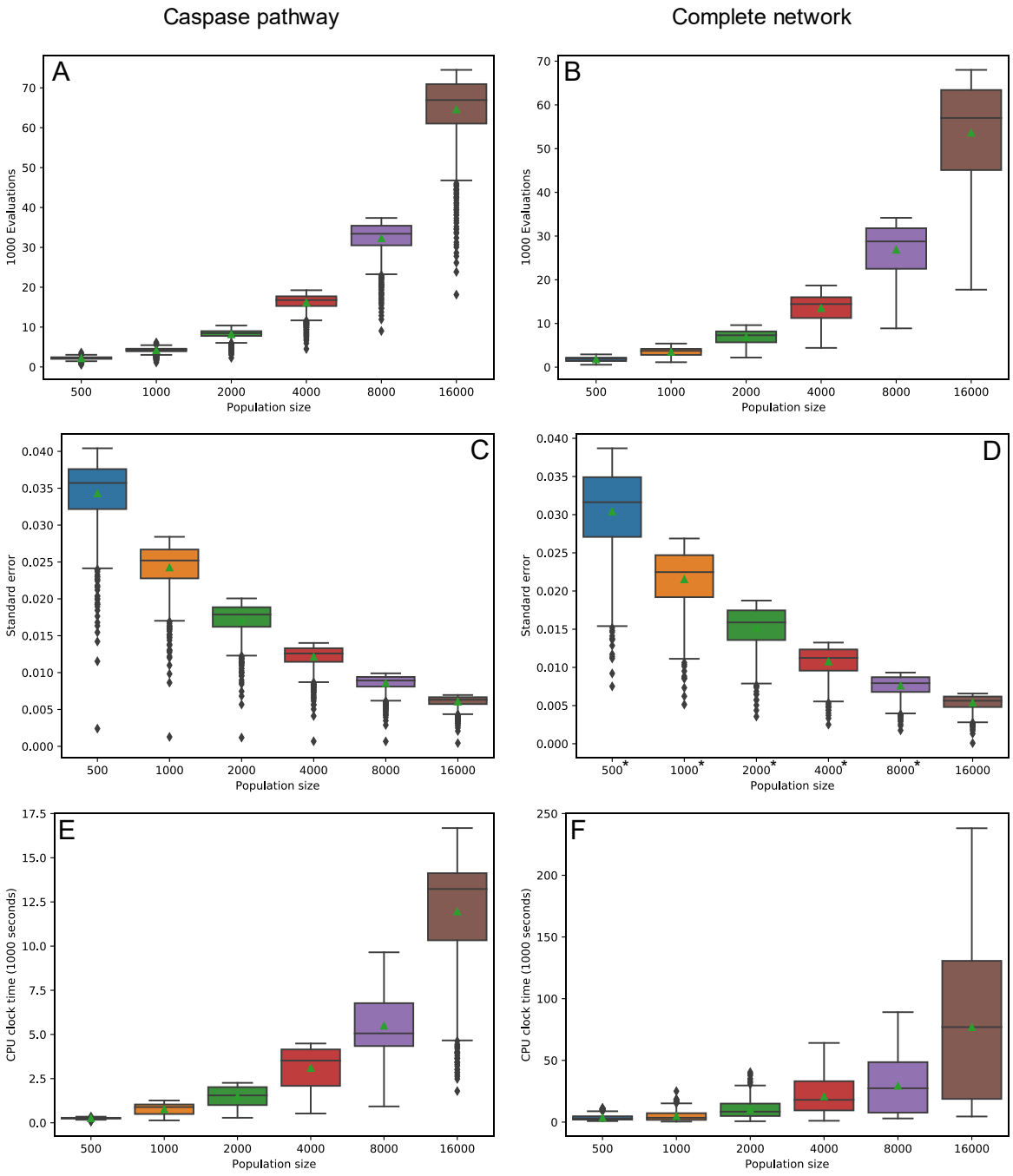

Figure 5. Precision vs. computational cost. (A) and (B) Average number of evaluations before termination of the MultiNest algorithm over a range of population sizes for the caspase pathway and complete network respectively. (C) and (D) Average of error estimates from MultiNest for each population size and the caspase and complete networks. (E) and (F) Average estimated CPU clock time over each population size for the caspase and complete networks respectively. *MultiNest was unable to estimate the error at Xiap = 0.

Discussion

Characterizing information flow in biological networks, the interactions between various pathways or network components, and shifts in phenotype upon regulatory perturbations is an exceedingly difficult task. Although comparative analysis of subnetwork regulation is possible with current computational methods, standard physicochemical modeling is highly dependent on a model's kinetic parameters and, unfortunately, parameters are typically unknown and must be calibrated to data that is often sparse. Any network inferences made with a particular set of parameters may be good *only* for that set of parameters because when data is lacking, different parameter sets that favor different network components may fit equally well. To overcome this limitation, we take a probabilistic approach to the inference of changes in network dynamics. The Bayesian evidence (expected value) is calculated for relevant subnetworks, with an objective function that quantifies an anticipated outcome, such as cell death, over an incrementing range of quantities for key regulators of the system in question. Differences in the trends in evidence for the subnetworks reveals information about their interactions and how they vary under regulatory changes. Alternatively, retaining the complete network while using objective functions that estimate the same quantity, such as pathway signal flux, but target different pathways can offer an alternative but complimentary view of changing network dynamics under regulatory perturbation.

There are several advantages to using this method over more traditional modeling. As model selection methods are *designed* for model comparison, they are a natural choice for the inference of differential response in subnetworks under changing regulatory conditions. Nested sampling is ideal when those pathways are modeled with physicochemical representations as the method provides a measure of robustness for attaining the desired outcome. The evidence calculation effectively integrates out the impact of parameters, so long as reasonable parameter ranges are chosen. This leaves the network topology and initial conditions as the remaining factors influencing pathway response from regulator perturbation. Lack of dependence on parameter calibration also obviates the need for the data to carry it out. Typically, model selection methods also require a fit to experimental data to select the best model candidate. Here though, we are not choosing a preferred model by comparison of a single evidence value for each one but instead, considering the relative *changes* in evidence values as a proxy for differential pathway response to regulatory changes. All that is required for such an analysis is a desired final model state or a functional process that can be estimated for a simulated run. Thus, although experimental data can certainly be used, it is not a requirement. In all, these properties allow for a head-to-head, topology-dependent, data-free comparison of subnetwork response to changes in regulatory conditions.

The utility of the method is evident when applied to the regulation of extrinsic apoptosis with the apoptosis inhibitor XIAP. By deconstructing the network into all relevant subnetworks and comparing the evidence trends of each of them, several insights/hypotheses were made. First, our results are in line with experimentation and the hypothesis that increasing XIAP, particularly from very low levels, puts the apoptotic system into a state that favors the Type II pathway. The diverging evidence trends between the isolated caspase pathway and both the mitochondrial pathway and the complete network imply that XIAP produces this state by

differentially suppressing the caspase pathway over networks that include the mitochondrial pathway, thus requiring mitochondrial amplification to achieve apoptosis. There also appears to be an optimal XIAP value for achieving the Type II phenotype at around 41,000 molecules per cell, as demonstrated by the trend in the Bayes factors between the caspase pathway and the complete network. Second, it appears that XIAP inhibition may be the primary mechanism by which mitochondrial amplification of the apoptotic signal is executed. This is illustrated by higher likelihood of apoptosis, at lower levels of XIAP, for the caspase plus XIAP inhibition network than for the caspase plus mitochondrial signal transduction or the mitochondrial signal transduction alone. This hypothesis is further supported by the estimated expected values for signal flux. The caspase pathway flux is consistently higher than that for the mitochondrial pathway indicating that it is more likely that the majority of the signal is passing through the caspase pathway. Finally, the lower trend for the complete network versus the mitochondrial pathway at lower values of XIAP, despite the additional pathway for apoptotic signaling contained in the complete network, suggests that the signal through the caspase pathway may get degraded under some narrow regulatory conditions, conditions that may be altered by the mitochondrial pathway to enable flow of the apoptotic signal through the caspase pathway. Given all these observations, a reasonable mechanistic hypothesis would be that under low signal throughput the caspase pathway acts as a sink until the amplified signal makes its way through the mitochondrial pathway. Inhibition of XIAP then allows the signal to pass through the caspase pathway, carrying the bulk of the apoptotic signal, but also through the mitochondrial induced apoptosome as a secondary route.

One limitation to using trends in Bayesian evidence for pathway or phenotype analysis is the computational cost. For example, the average estimated clock time of 76,981 seconds for the complete network under the PARP cleavage objective function and at a population size of 16,000 equates to nearly 714 CPU days for that entire run. Although the run time for evidence calculation can vary greatly it is correlated to the size of the model as was seen with the equivalent caspase pathway run at an average of 11,964 seconds. Fortunately, reducing the resolution (the number of sets of initial values for which an evidence value is estimated) and the precision (the population size) can drastically reduce the cost and in many cases the method will still be viable. The chosen objective function can also have a significant effect on the run time. The precision of the flux-based evidence landscapes was reduced by 75% for this reason. One aspect of the method that is severely restrictive is the number of model components that can be varied in the same run since the computational cost increases exponentially with each additional variable. Another consideration is the interpretation of results. The evidence and Bayes factor landscapes provide an abstract view of how the subnetworks respond to perturbations of their components, the meaning of which must be deduced in the context of the networks they represent and the objective function that generated them.

Conclusions

Trends in the Bayesian evidence for pathways in a biological network under regulatory perturbations provide a probabilistic approach to the analysis of pathway dynamics, the interplay between them, and the differential effects on them as regulatory conditions change. The method effectively removes the dependence on calibrated parameters, leaving model topology and initial conditions as the primary driver of pathway response to changes in protein concentration. In this work we used the method to evaluate the mechanisms underpinning apoptotic signal execution and the transition from a Type I to Type II apoptotic phenotype in the extrinsic apoptosis network. We found that while XIAP has an inhibitory effect on both the caspase and mitochondrial pathways, it disproportionally affects the caspase pathway, thus requiring mitochondrial amplification. There also appears to be an optimal level of XIAP for achieving a Type II phenotype, after which the system likely tends toward complete resistance to apoptosis. Mitochondrial amplification appears to primarily take the form of inhibition of XIAP and the abatement of signal inhibition through the caspase pathway, with direct signaling through the mitochondrial pathway a secondary mechanism. Without amplification the caspase pathway may very well be a sink for the apoptotic signal. Overall, these computational results confirm the experimental results regarding XIAP and its regulation of extrinsic apoptosis but also suggest the mechanisms that effect that regulation and provides insight into the crosstalk between the caspase and the mitochondrial pathway.

Construction and comparison of Bayesian evidence trends is a powerful approach to the analysis of network dynamics, particularly when experimental data is sparse. Each comparison lends additional insights that can be built into an overall hypothesis for the causal mechanisms of changes in network dynamics under regulatory perturbation. Such a probabilistic approach to systems biology may prove to be a valuable tool going forward.

Acknowledgements

This work was supported by the NIH NCI U01CA215845 (CFL), as well as NSF MCB 1411482 (CFL) We thank the Incyte-Vanderbilt Alliance (CFL) for their support of this project. We also thank the Advanced Computing Center for Research and Education (ACCRE) for computational resources and support needed to complete this work. Finally, we extend our thanks to Dr Blake Wilson for his effort in reviewing this work and providing feedback.

References

1. Loscalzo J, Barabasi A-L. Systems biology and the future of medicine. Wiley Interdisciplinary Reviews: Systems Biology and Medicine. 2011;3(6):619–27..

2. Bhalla US, Iyengar R. Emergent Properties of Networks of Biological Signaling Pathways. Science. 1999 Jan 15;283(5400):381–7.

3. Kitano H. Computational systems biology. Nature. 2002 Nov;420(6912):206.

4. Aldridge BB, Gaudet S, Lauffenburger DA, Sorger PK. Lyapunov exponents and phase diagrams reveal multi-factorial control over TRAIL-induced apoptosis. Molecular Systems Biology. 2011 Jan 1;7(1):553.

5. Raychaudhuri S, Raychaudhuri SC. Monte Carlo Study Elucidates the Type 1/Type 2 Choice in Apoptotic Death Signaling in Healthy and Cancer Cells. Cells. 2013 Jun;2(2):361–92.

6. Riel V, A.w N. Dynamic modelling and analysis of biochemical networks: mechanism-based models and model-based experiments. Brief Bioinform. 2006 Dec 1;7(4):364–74.

7. Shockley EM, Vrugt JA, Lopez CF. PyDREAM: high-dimensional parameter inference for biological models in python. Bioinformatics. 2018 Feb 15;34(4):695–7.

8. Burnham KP, Anderson DR. Model Selection and Multimodel Inference: A Practical Information-Theoretic Approach [Internet]. 2nd ed. New York: Springer-Verlag; 2002 [cited 2019 Apr 24]. Available from: https://www.springer.com/us/book/9780387953649

9. Symonds MRE, Moussalli A. A brief guide to model selection, multimodel inference and model averaging in behavioural ecology using Akaike's information criterion. Behav Ecol Sociobiol. 2011 Jan 1;65(1):13–21.

10. Akaike H. Information Theory and an Extension of the Maximum Likelihood Principle. In: Parzen E, Tanabe K, Kitagawa G, editors. Selected Papers of Hirotugu Akaike [Internet]. New York, NY: Springer New York; 1998 [cited 2019 May 14]. p. 199–213. (Springer Series in Statistics). Available from: https://doi.org/10.1007/978-1-4612-1694-0_15

11. Schwarz G. Estimating the Dimension of a Model. Ann Statist. 1978 Mar;6(2):461–4.

12. Eydgahi H, Chen WW, Muhlich JL, Vitkup D, Tsitsiklis JN, Sorger PK. Properties of cell death models calibrated and compared using Bayesian approaches. Molecular Systems Biology. 2013 Jan 1;9(1):644.

13. Lartillot N, Philippe H. Computing Bayes Factors Using Thermodynamic Integration. Syst Biol. 2006 Apr 1;55(2):195–207.

14. Skilling J. Nested sampling for general Bayesian computation. Bayesian Anal. 2006 Dec;1(4):833–59.

15. Feroz F, Hobson MP, Bridges M. MultiNest: an efficient and robust Bayesian inference tool for cosmology and particle physics. Mon Not R Astron Soc. 2009 Oct 1;398(4):1601–14.

16. Feroz F, Hobson MP, Cameron E, Pettitt AN. Importance Nested Sampling and the MultiNest Algorithm. arXiv:13062144 [astro-ph, physics:physics, stat] [Internet]. 2013 Jun 10 [cited 2019 May 14]; Available from: http://arxiv.org/abs/1306.2144

17. Lopez CF, Muhlich JL, Bachman JA, Sorger PK. Programming biological models in Python using PySB. Molecular Systems Biology. 2013 Jan 1;9(1):646.

18. Spencer SL, Gaudet S, Albeck JG, Burke JM, Sorger PK. Non-genetic origins of cell-to-cell variability in TRAIL-induced apoptosis. Nature. 2009 May;459(7245):428–32.

19. Buchner J, Georgakakis A, Nandra K, Hsu L, Rangel C, Brightman M, et al. X-ray spectral modelling of the AGN obscuring region in the CDFS: Bayesian model selection and catalogue. A&A. 2014 Apr 1;564:A125.

20. Mitra ED, Dias R, Posner RG, Hlavacek WS. Using both qualitative and quantitative data in parameter identification for systems biology models. Nature Communications. 2018 Sep 25;9(1):3901.

21. Shockley EM, Rouzer CA, Marnett LJ, Deeds EJ, Lopez CF. Signal integration and information transfer in an allosterically regulated network. bioRxiv. 2019 Jan 11;518514. ACCEPTED IN NPJ Systems Biology & Applications 2019

22. Aldridge BB, Burke JM, Lauffenburger DA, Sorger PK. Physicochemical modelling of cell signalling pathways. Nature Cell Biology. 2006 Nov;8(11):1195.

23. Dai H, Ding H, Peterson KL, Meng XW, Schneider PA, Knorr KLB, et al. Measurement of BH3-only protein tolerance. Cell Death and Differentation. 2018 Jan 1;25(2):282–93.

24. Eissing T, Conzelmann H, Gilles ED, Allgöwer F, Bullinger E, Scheurich P. Bistability Analyses of a Caspase Activation Model for Receptor-induced Apoptosis. J Biol Chem. 2004 Aug 27;279(35):36892–7.

25. Aitken S, Akman OE. Nested sampling for parameter inference in systems biology: application to an exemplar circadian model. BMC Systems Biology. 2013 Jul 30;7(1):72.

26. Pullen N, Morris RJ. Bayesian Model Comparison and Parameter Inference in Systems Biology Using Nested Sampling. PLOS ONE. 2014 Feb 11;9(2):e88419.

27. Xu T-R, Vyshemirsky V, Gormand A, Kriegsheim A von, Girolami M, Baillie GS, et al. Inferring Signaling Pathway Topologies from Multiple Perturbation Measurements of Specific Biochemical Species. Sci Signal. 2010 Mar 16;3(113):ra20–ra20.

28. Ashkenazi A, Dixit VM. Death Receptors: Signaling and Modulation. Science. 1998 Aug 28;281(5381):1305–8.

29. Boldin MP, Varfolomeev EE, Pancer Z, Mett IL, Camonis JH, Wallach D. A Novel Protein That Interacts with the Death Domain of Fas/APO1 Contains a Sequence Motif Related to the Death Domain. J Biol Chem. 1995 Apr 7;270(14):7795–8.

30. Kischkel FC, Lawrence DA, Chuntharapai A, Schow P, Kim KJ, Ashkenazi A. Apo2L/TRAIL-

Dependent Recruitment of Endogenous FADD and Caspase-8 to Death Receptors 4 and 5. Immunity. 2000 Jun 1;12(6):611–20.

31. Sprick MR, Weigand MA, Rieser E, Rauch CT, Juo P, Blenis J, et al. FADD/MORT1 and Caspase-8 Are Recruited to TRAIL Receptors 1 and 2 and Are Essential for Apoptosis Mediated by TRAIL Receptor 2. Immunity. 2000 Jun 1;12(6):599–609.

32. Krueger A, Schmitz I, Baumann S, Krammer PH, Kirchhoff S. Cellular FLICE-inhibitory Protein Splice Variants Inhibit Different Steps of Caspase-8 Activation at the CD95 Death-inducing Signaling Complex. J Biol Chem. 2001 Jun 8;276(23):20633–40.

33. Salvesen GS, Dixit VM. Caspase activation: the induced-proximity model. Proc Natl Acad Sci U S A. 1999 Sep;96(20):10964–7.

34. Martin DA, Siegel RM, Zheng L, Lenardo MJ. Membrane Oligomerization and Cleavage Activates the Caspase-8 (FLICE/MACHα1) Death Signal. J Biol Chem. 1998 Feb 20;273(8):4345–9.

35. Boatright KM, Salvesen GS. Mechanisms of caspase activation. Current Opinion in Cell Biology. 2003 Dec 1;15(6):725–31.

36. Stennicke HR, Jürgensmeier JM, Shin H, Deveraux Q, Wolf BB, Yang X, et al. Pro-caspase-3 Is a Major Physiologic Target of Caspase-8. J Biol Chem. 1998 Oct 16;273(42):27084–90.

37. Li H, Zhu H, Xu C, Yuan J. Cleavage of BID by Caspase 8 Mediates the Mitochondrial Damage in the Fas Pathway of Apoptosis. Cell. 1998 Aug 21;94(4):491–501.

38. Luo X, Budihardjo I, Zou H, Slaughter C, Wang X. Bid, a Bcl2 Interacting Protein, Mediates Cytochrome c Release from Mitochondria in Response to Activation of Cell Surface Death Receptors. Cell. 1998 Aug 21;94(4):481–90.

39. Desagher S, Osen-Sand A, Nichols A, Eskes R, Montessuit S, Lauper S, et al. Bid-induced Conformational Change of Bax Is Responsible for Mitochondrial Cytochrome c Release during Apoptosis. The Journal of Cell Biology. 1999 Mar 8;144(5):891–901.

40. Kelekar A, Thompson CB. Bcl-2-family proteins: the role of the BH3 domain in apoptosis. Trends in Cell Biology. 1998 Aug 1;8(8):324–30.

41. Oltval ZN, Milliman CL, Korsmeyer SJ. Bcl-2 heterodimerizes in vivo with a conserved homolog, Bax, that accelerates programed cell death. Cell. 1993 Aug 27;74(4):609–19.

42. Leber B, Lin J, Andrews DW. Embedded together: The life and death consequences of interaction of the Bcl-2 family with membranes. Apoptosis. 2007 May 1;12(5):897–911.

43. Letai A, Bassik MC, Walensky LD, Sorcinelli MD, Weiler S, Korsmeyer SJ. Distinct BH3 domains either sensitize or activate mitochondrial apoptosis, serving as prototype cancer therapeutics. Cancer Cell. 2002 Sep 1;2(3):183–92.

44. Yang E, Zha J, Jockel J, Boise LH, Thompson CB, Korsmeyer SJ. Bad, a heterodimeric partner for Bcl-XL and Bcl-2, displaces Bax and promotes cell death. Cell. 1995 Jan 27;80(2):285–91.

45. Kale J, Osterlund EJ, Andrews DW. BCL-2 family proteins: changing partners in the dance towards death. Cell Death and Differentiation. 2018 Jan;25(1):65–80.

46. Tewari M, Quan LT, O'Rourke K, Desnoyers S, Zeng Z, Beidler DR, et al. Yama/CPP32β, a mammalian homolog of CED-3, is a CrmA-inhibitable protease that cleaves the death substrate poly(ADP-ribose) polymerase. Cell. 1995 Jun 2;81(5):801–9.

47. Nicholson DW, Ali A, Thornberry NA, Vaillancourt JP, Ding CK, Gallant M, et al. Identification and inhibition of the ICE/CED-3 protease necessary for mammalian apoptosis. Nature. 1995 Jul;376(6535):37.

48. Jost PJ, Grabow S, Gray D, McKenzie MD, Nachbur U, Huang DCS, et al. XIAP discriminates between type I and type II FAS-induced apoptosis. Nature. 2009 Aug;460(7258):1035–9.

49. Huang Y, Park YC, Rich RL, Segal D, Myszka DG, Wu H. Structural Basis of Caspase Inhibition by XIAP: Differential Roles of the Linker versus the BIR Domain. Cell. 2001 Mar 9;104(5):781–90.

50. Suzuki Y, Nakabayashi Y, Takahashi R. Ubiquitin-protein ligase activity of X-linked inhibitor of apoptosis protein promotes proteasomal degradation of caspase-3 and enhances its anti-apoptotic effect in Fas-induced cell death. Proc Natl Acad Sci USA. 2001 Jul 17;98(15):8662–7.

51. Shiozaki EN, Chai J, Rigotti DJ, Riedl SJ, Li P, Srinivasula SM, et al. Mechanism of XIAP-Mediated Inhibition of Caspase-9. Molecular Cell. 2003 Feb 1;11(2):519–27.

52. Zou H, Li Y, Liu X, Wang X. An APAF-1·Cytochrome c Multimeric Complex Is a Functional Apoptosome That Activates Procaspase-9. J Biol Chem. 1999 Apr 23;274(17):11549–56.

53. Adrain C, Creagh EM, Martin SJ. Apoptosis-associated release of Smac/DIABLO from mitochondria requires active caspases and is blocked by Bcl-2. The EMBO Journal. 2001 Dec 3;20(23):6627–36.

54. Cowling V, Downward J. Caspase-6 is the direct activator of caspase-8 in the cytochrome c -induced apoptosis pathway: absolute requirement for removal of caspase-6 prodomain. Cell Death & Differentiation. 2002 Oct;9(10):1046.

55. Ku B, Liang C, Jung JU, Oh B-H. Evidence that inhibition of BAX activation by BCL-2 involves its tight and preferential interaction with the BH3 domain of BAX. Cell Research. 2011 Apr;21(4):627–41.

56. Handley WJ, Hobson MP, Lasenby AN. PolyChord: next-generation nested sampling. Mon Not R Astron Soc. 2015 Nov 11;453(4):4385–99.